ONE-WAY WAVE PROPAGATORS FOR VELOCITY ANALYSIS ON CURVILINEAR COORDINATES

SCOTT BURDICK, ROBERT D. VAN DER HILST, AND MAARTEN V. DE HOOP

Earth Resources Laboratory
Department of Earth, Atmospheric and Planetary Sciences
Massachusetts Institute of Technology
Cambridge, MA 02139

1. abstract

Due to present computational limitations, migration by the one-way wave equation remains an integral tool in seismic exploration. For the realistic interpretation of common image point gathers, it is necessary that migration be free from artifacts from caustics and turning waves. In order to permit situations where turning waves occur, we perform our migration on specially chosen curvilinear coordinates where waves do not travel horizontally. We present an implementation of the curvilinear one-way wave equation using a rational approximation and discuss its application in migration velocity analysis, as well as transmission and reflection tomography.

2. Introduction

In migration of reflected data and migration velocity analysis (MVA), it is vital that common image gathers are free from artifacts due to caustics and turning waves. Downward continuation of surface data using one-way wave propagation methods does not allow for the possibility of wavefronts traveling horizontally or overturning. If we wish to investigate situations where turning waves occur, such as overturned faults or salt flanks while still taking advantage of fast, accurate one-way propagators, we must carry out our migration in a curvilinear coordinate system. We define curvilinear coordinates suited to a particular tectonic or geological setting based on a pseudodepth direction in which the waves of interest propagate, as opposed to using coordinates generated by the rays associated with propagation (Sava and Fomel, 2005). The hyperbolic one-way wave equation can then be derived in the new coordinate system starting from the variation principle, then cast into a computationally efficient thin-slab propagator based on the rational approximation.

In addition to general application to migration problems, we develop our propagator specifically with differential semblance velocity analysis in mind. Analysis using wave-equation angle transform annihilators as the semblance criteria (de Hoop et al., 2006) has the advantage that it can be used to estimate the reflection coefficient induced by the background velocity, and remains artifact free in the presence of caustics. To expand its applicability, a curvilinear angle transform has been developed (Stolk and de Hoop, 2007) in order to allow for MVA in the presence of turning waves as well as caustics.

The generalization of the one-way wave equation into curvilinear coordinates makes it possible, furthermore, to apply our fast, accurate propagation method to a broad suite of seismic techniques. The ability to handle turning waves makes it possible to use the same computational framework for problems ranging from transmission tomography from local microseismicity to

reflection tomography using underside and free surface reflections. A change of coordinates also makes it possible to apply migration methods to global seismology problems where the curvature of the Earth cannot be ignored.

Transforming the one-way wave equation

In order to take advantage of fast, accurate one-way propagators, we require that the waves travel nowhere horizontally before encountering a scattering point. To accommodate situations such as salt flank reflections or turning waves in strongly heterogeneous media, we transform the one-way wave equation into curvilinear coordinates.

The curvilinear coordinate system is denoted by $\tilde{x} = \tilde{x}(x,z), \tilde{z} = \tilde{z}(x,z)$. The pseudodepth coordinate, $\tilde{z}$ is required to be orthogonal to the other coordinates. The Riemannian transformation metric is given by

$$\tilde{g}_{il} = \frac{\partial(x,z)^j}{\partial(\tilde{x},\tilde{z})^i}\delta_{jk}\frac{\partial(x,z)^k}{\partial(\tilde{x},\tilde{z})^l} \tag{1}$$

where we sum over repeated indices. The inverse metric is given as $\tilde{g}^{il}$. To obtain an accurate acoustic wave equation in this coordinate system, the transformation begins at the variational formula. The wave equation is derived, as in Stolk and de Hoop (2007), by transforming the action functional into curvilinear coordinates according to the Riemannian metric and perturbing it to find the Euler-Lagrange equations.

After transforming into the frequency domain, we define the curvilinear wavefield as $\tilde{U}(\tilde{x},\tilde{z},\omega) = U(x(\tilde{x},\tilde{z}), z(\tilde{x},\tilde{z}), \omega)$. We write the resulting wave equation as a first-order system in $\tilde{z}$. With $\alpha = \rho^{-1}\tilde{g}^{33}\left|\frac{\partial(x,z)}{\partial(\tilde{x},\tilde{z})}\right|$:

$$\left(\frac{\partial}{\partial\tilde{z}} - i\omega A\right)\begin{pmatrix}\tilde{U}\\ -i\omega^{-1}\alpha\frac{\partial\tilde{U}}{\partial\tilde{z}}\end{pmatrix} = \begin{pmatrix}0\\ f\left|\frac{\partial(x,z)}{\partial(\tilde{x},\tilde{z})}\right|\end{pmatrix} \tag{2}$$

where

$$A = \begin{pmatrix}0 & \alpha^{-1}\\ \kappa\left|\frac{\partial(x,z)}{\partial(\tilde{x},\tilde{z})}\right| + \omega^{-2}\frac{\partial}{\partial\tilde{x}}\rho^{-1}\left|\frac{\partial(x,z)}{\partial(\tilde{x},\tilde{z})}\right|\tilde{g}^{33}\frac{\partial}{\partial\tilde{x}} & 0\end{pmatrix} \tag{3}$$

This allows us to derive the one-way wave equation by finding the eigenvectors of the system. The result is a transformation of variables $(\tilde{U}, -i\omega^{-1}\alpha\frac{\partial\tilde{U}}{\partial\tilde{z}}) \to (\tilde{U}_+, \tilde{U}_-)$ such that the upgoing and downgoing constituents of the wavefield, $\tilde{U}_+$ and $\tilde{U}_-$, conserve acoustic power flux. The one-way wave equation is then

$$\frac{\partial}{\partial\tilde{z}}\tilde{U}_\pm \mp i\omega\Gamma\tilde{U}_\pm = f_\pm \tag{4}$$

where the pseudodifferential vertical slowness operator, defined as the square root of the A operator, $\Gamma = (A_{12}^{1/2}A_{21}A_{12}^{1/2})^{1/2}$ (with $c^{-2} = \rho\kappa$) is given by

$$\Gamma = \sqrt{c^{-2}\tilde{g}_{33} + \omega^{-2}\frac{\partial}{\partial\tilde{x}}\tilde{g}^{11}\tilde{g}_{33}\frac{\partial}{\partial\tilde{x}}} \tag{5}$$

In order to ensure the correct amplitude for one-way propagation, the subprinciple symbol should also be included. For the purposes of this abstract, we will consider one-way propagation in two dimensions, but the derivation extends easily to three dimensions.

3. Rational approximation propagator

From a number of numerical approximations of the square root operator, we proceed via the rational approximation for its high angle accuracy and extendibility to three dimensions. We generalize the method of van Stralen et al. (1998) for use in curvilinear coordinates. Using the rational approximation, we seek to express the square root operator as the quotient of two polynomials. For the desired angular accuracy, we extend the series in the numerator to the second degree and the series in the denominator to the first degree. Defining $\Xi \equiv -\tilde{g}_{33}^{-1}\frac{c}{\omega^2}\frac{\partial}{\partial\tilde{x}}\tilde{g}^{11}\tilde{g}_{33}\frac{\partial}{\partial\tilde{x}}c$, we have the self-adjoint

$$\begin{aligned}\Gamma &= \sqrt{\frac{\tilde{g}_{33}}{c}}\sqrt{1+\Xi}\frac{1}{\sqrt{c}} \\ &\approx \sqrt{\frac{\tilde{g}_{33}}{c}}\left(1+[1+\beta_3\Xi]^{-1}[\beta_1\Xi+\beta_2\Xi^2]\right)\frac{1}{\sqrt{c}}\end{aligned} \tag{6}$$

We find the coefficients to be $\beta_1 = 1/2, \beta_2 = 1/8, \beta_3 = 1/2$. The computational cost of the resulting algorithm is primarily due to the inversion of one tridiagonal matrix and one 5-diagonal matrix. We add additional accuracy at no additional cost by using an implicit implementation of the approximate Laplace operator.

$$\langle\Xi\rangle = (1+a\Delta\tilde{x}^2\Xi_{cent})^{-1}\Xi_{cent} \tag{7}$$

where Ξ_{cent} is the central difference discretization of Ξ in $\tilde{x}$. From the Taylor expansion, the value $a = 1/12$ is found. Next, in order to further improve computational accuracy and reduce discretization artifacts, we shift Γ into the comoving frame of reference. With τ equal to the integral of slowness between the boundary and depth of propagation, Γ becomes:

$$\Gamma \approx e^{i\omega\tau}\sqrt{\frac{\tilde{g}_{33}}{c}}\left[1+\beta_3\langle\Xi\rangle\right]^{-1}\left[\beta_1\langle\Xi\rangle+\beta_2\langle\Xi\rangle^2\right]\sqrt{\frac{1}{c}}e^{-i\omega\tau} \tag{8}$$

With this approximation of the square root equation, we develop a thin slab propagator. The product integral solution of Eq. (4) can be approximated with another (1,1) rational approximation, which leads to a Crank-Nicholson finite difference scheme, accurate up to order $\Delta\tilde{z}^3$.

$$\begin{aligned}\tilde{U}(\tilde{x},\tilde{z}+\Delta\tilde{z}) &\approx e^{-i\omega\Delta\tilde{z}\Gamma(\tilde{x},\tilde{z}+\frac{1}{2}\Delta\tilde{z})}\tilde{U}(\tilde{x},\tilde{z}) \\ &\approx \frac{1-i\omega\Delta\tilde{z}\beta_4\Gamma}{1+i\omega\Delta\tilde{z}\beta_4\Gamma}\tilde{U}(\tilde{x},\tilde{z})\end{aligned} \tag{9}$$

To further improve the angular accuracy of propagation, β_1, β_2, β_3, β_4, and a can be optimized. Denoting γ as the symbol of the square root slowness operator, we minimize the differences between the slowness operator and the group slowness of the approximate operator, γ_{group}, and the difference between the group slowness and phase slowness, γ_{phase}. Numerical

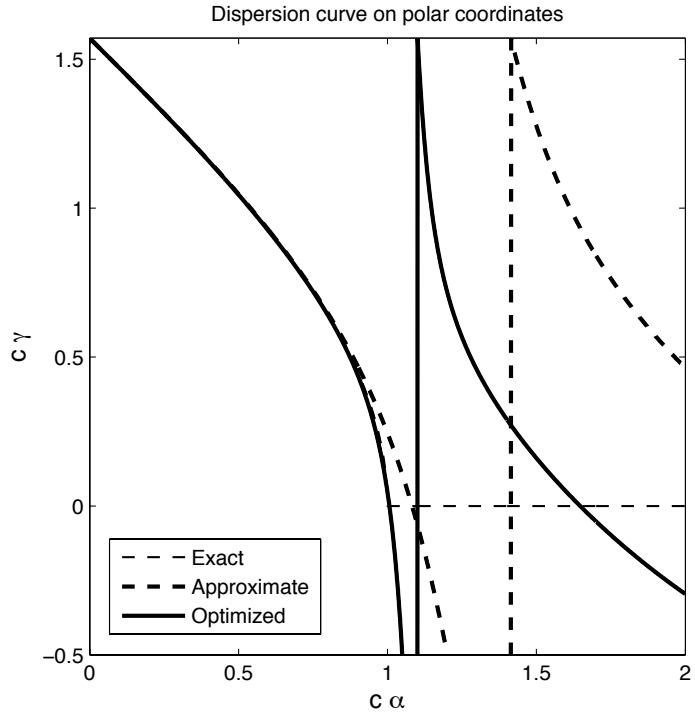

FIGURE 1. Comparison of dispersion curves for rational approximation (dashed) versus optimized parameters (solid), with α as the pseudodifferential symbol of Ξ. The optimized curve plots on top of the exact curve, demonstrating the high angular accuracy. Plotted in polar coordinates with $\theta = 0$.

anisotropy is given by $\gamma_{group} - \gamma$ and $\gamma_{phase} - \gamma_{group}$ gives the numerical dispersion. The optimized coefficients are $\beta_1 = 0..486, \beta_2 = 0.349, \beta_3 = 0.841, \beta_4 = 0.529$ and $a = 0.114$. Figure 1 shows the effect of the optimized parameters on the shape of the dispersion curve compared to the analytically determined parameters.

Further improvements can be made in the suppression of approximation artifacts caused by postcritically propagating modes if we allow the parameters and frequency to be complex. This results in an amplification factor that is near unity for less than the critical value and tapers off beyond it.

3.1. **Perfectly matched layers.** To prevent nonphysical reflections from the boundaries of the computational grid, it is necessary to use an absorbing boundary condition. Perfectly matched layers (PML) based on Collino (1997) were put into place on both $\tilde{x}$ boundaries. The PML is achieved by complexifying the Laplacian operator in the region where damping occurs.

$$\Xi \to -\tilde{g}_{33}^{-1} \frac{c}{\omega^2} \frac{i\omega}{i\omega + \sigma} \frac{\partial}{\partial \tilde{x}} \tilde{g}^{11} \tilde{g}_{33} \frac{i\omega}{i\omega + \sigma} \frac{\partial}{\partial \tilde{x}} c \tag{10}$$

where $\sigma(\tilde{x}) = 0$ in the freely propagating medium and is determined to create the weakest reflection. Figure 2 demonstrates the results of the propagator with perfectly matched layers on polar coordinates, $\tilde{x} = r = \sqrt{x^2 + z^2}, \tilde{z} = \theta = \arctan(\frac{z}{x})$.

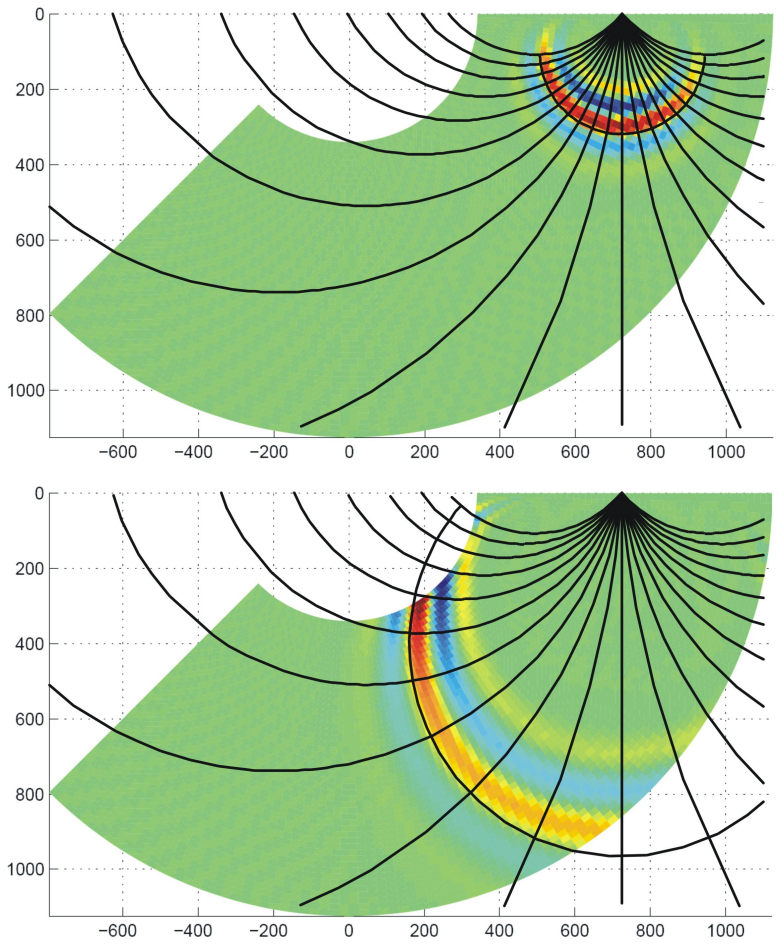

FIGURE 2. Overturning wave in the wavespeed model shown in **??**. Rays and wavefront are projected on top of the wave, demonstrating the accuracy of propagation in overturning coordinates. Distances are in meters.

4. APPLICATIONS

4.1. **Transmission tomography.** Although we develop our propagator with migration velocity analysis in mind, the general framework has possible application to numerous exploration problems. The generalization of the one-way wave equation on curvilinear coordinates makes it possible to apply our propagation method to transmission studies. Using a polar coordinate system with θ ranging from 0 to π, it is possible to model a large offset transmission survey. In cases like this, it is vital to ensure the computational grid size at the outer radius meets the Nyquist criterion. It may be prudent to carry out propagation on a variable-size grid with sections of smaller $d\theta$ at greater radius. Regions requiring grid refinements could be determined through wavefront construction. Similar methodology could be applied more easily to surveys with surface sources and receivers at depth or crosshole surveys, as in figure 3. Although a global scale crosshole experiment is implausible, the example illustrates the easy applicability of our method to global seismology on a spheroidal Earth.

Passive seismics are becoming a useful tool in geophysical exploration. Using microseismicity caused by local tectonism or reservoir-induced earthquakes, wave-equation transmission tomography can be performed. Figures 4 shows sensitivity kernels for an overturning wave produced

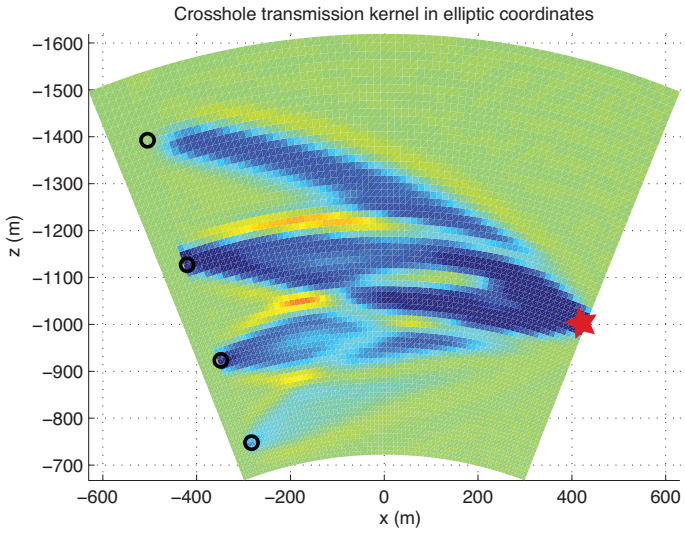

FIGURE 3. Transmission kernel for crosshole survey in elliptic coordinates, $\tilde{x} = a\cosh(x)\cos(z), \tilde{z} = a\sinh(x)\sin(z)$. Source (star) is recorded at four geophones (black dots) at the left.

at depth and recorded at a single geophone at the surface. The formation of the kernel in polar coordinates is achieved using the seismic adjoint method. The source function was correlated with the second time derivative of the back-propagated data to determine the region of the model that is sensitive to, in this case, changes in density. Using waveform mismatch as the adjoint source, the model gradient can be determined for density and other acoustic parameters, and a tomographic inversion can be performed (Tromp et al., 2005).

4.2. **Migration velocity analysis.** We develop our wave-equation angle transform for the purpose of performing migration velocity analysis on reflection data recorded at the surface, $\tilde{z} = 0$. Figure 5 shows reflection data, $d(\tilde{x}_r, t, \tilde{x}_s)$, being migrated in the pseudodepth coordinate using the rational one-way propagator. The source function is propagated downward as well, and the two are correlated, yielding the subsurface wavefield in midpoint-offset coordinates, $(\tilde{x}, \tilde{h}_x, \tilde{z}, \tilde{h}_z = 0)$, where the offset is contained on a level-set of the pseudodepth function.

For reflection tomography, instead of applying the normal imaging condition, $I(\tilde{x}, \tilde{z}) = \tilde{u}(\tilde{x} - \frac{\tilde{h}_x}{2}, \tilde{x} + \frac{\tilde{h}_x}{2}, t, \tilde{z})|_{\tilde{h}_x=0, t=0}$, to the downward continued wavefield, a curvilinear angle transform, $\mathcal{A}$, is applied to create an image $I(\tilde{x}, \tilde{z}, \tilde{p})$. With this angle-transformed data, we can define our semblance criteria. If the data has been migrated through an acceptable background velocity, the common image-point gathers should be independent of $\tilde{p}$. We can therefore describe curvilinear annihilators to evaluate whether the velocity model is acceptable for modeling the observed data. The annihilator, W, is fundamentally

a derivative in $\tilde{p}$. For an acceptable background model, $Wd = 0$. Combined with its adjoint, this will give us the criteria for evaluating model quality and allow us to optimize the model by minimizing the effect of the annihilators on the data. The problem can then be cast as an adjoint method problem and solved via conjugate gradient.

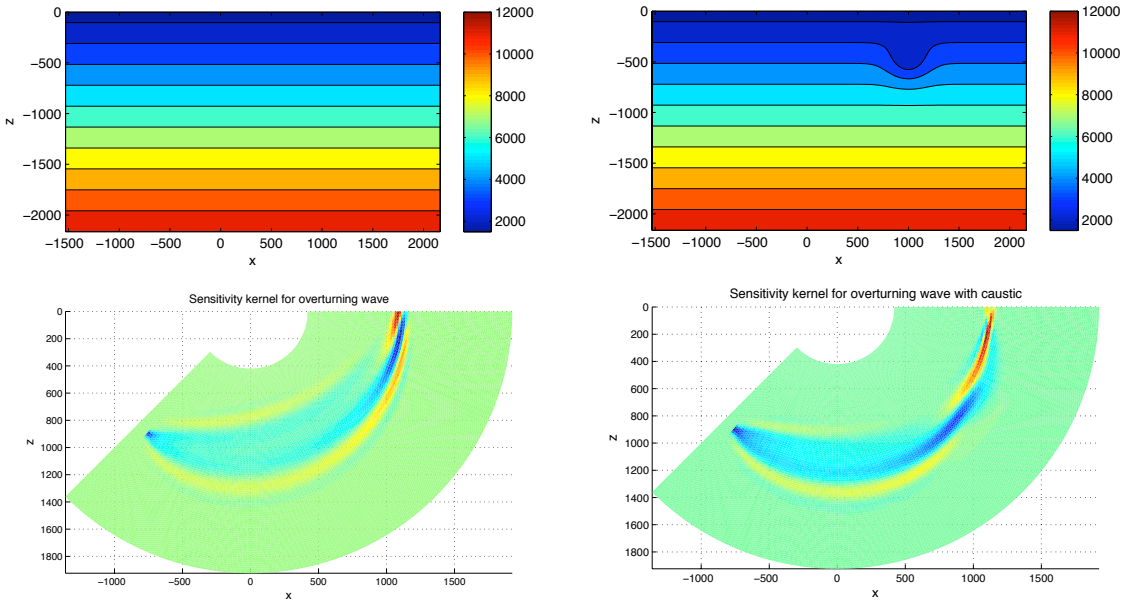

FIGURE 4. (a) Wavespeed model with gradient in z. (b) Similar to wavespeed model in (a) with a $-1500m/s$ Gaussian lens added. (c) Density kernel for shot/geophone pair in model (a). Note the appearance of the famous banana-doughnut shape. (d) Sensitivity kernel for model in (b) demonstrating both caustics and overturning rays. The development of the caustics causes the kernel to distort.

5. CONCLUSION

We have developed a technique for one-way wave propagation on curvilinear coordinates using a rational approximation. This approximation yields high angular accuracy with only a few terms in the expansion, therefore allowing for accurate propagation at relatively low computational expense. The generalization of the one-way equation extends the application of migration and migration velocity analysis to a broad array of complex environments and survey geometries.

REFERENCES

Collino, F., 1997, Perfectly matched absorbing layers for the paraxial equations: Journal of Computational Physics, **131**, 164–180.

de Hoop, M. V., R. D. van der Hilst, and P. Shen, 2006, Wave-equation reflection tomography: annihilators and sensitivity kernels: Geophysical Journal International, **167**, 1332–1352.

Sava, P. and S. Fomel, 2005, Riemannian wavefield extrapolation: Geophysics, **70**, 45–56.

Stolk, C. C. and M. V. de Hoop, 2007, Curvilinear wave-equation angle transforms: Caustics, turning rays, absence of kinematic artifacts: Presented at the 77th Annual Meeting, Society of Exploration Geophysicists, Tulsa, Oklahoma.

Tromp, J., C. Tape, and Q. Y. Liu, 2005, Seismic tomography, adjoint methods, time reversal and banana-doughnut kernels: Geophysical Journal International, **160**, 195–216.

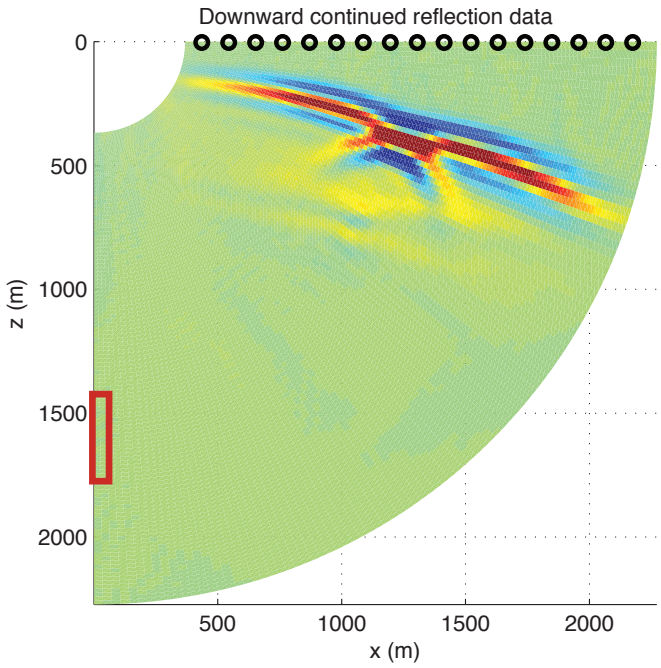

FIGURE 5. Reflection data generated with a full-wave finite difference program is downward continued in curvilinear coordinates as the first step towards migration velocity analysis. Waves from a surface source pass through a Gaussian lens then are reflected at a scatterer (red box) before being recorded at geophones (black circles).

van Stralen, M. J. N., M. V. de Hoop, and H. Block, 1998, Generalized Bremmer series with rational approximation for the scattering of waves in inhomogeneous media: Journal of Acoustic Society of America, **104**, 1943–1963.